

Monte-Carlo Study of the (102°,90°) Physics Optics for LEP

John M. Jowett

25 November 1997

Abstract

A new physics optics with phase advances $\mu_x = 102^\circ$ and $\mu_y = 90^\circ$ in the arc cells was recently tested in LEP. This note summarises the main results from the optics evaluation procedure that is now routinely applied to new LEP optics. This includes the study of the orbits, optics and dynamic apertures of an ensemble of imperfect machines with corrections similar to those applied in

Introduction

To evaluate the potential performance of a new optics for LEP, it is necessary to perform calculations of orbits, optics, beam parameters and dynamic apertures on an ensemble of imperfect machines. Over the last few years, a standard procedure has evolved for this purpose. For the present note, it has been applied to a "squeezed" (102°,90°) optics at 91.5 GeV. This optics is very similar to the optics that was subsequently tested in operation (the differences are discussed in Section 1.2).

The procedure followed is briefly outlined in the following subsection. Full technical details of the methods and computations will be published elsewhere. Only a selection of the most relevant results is presented in this note. Many others can be extracted from the database generated by the evaluation procedure.

1.1 Outline of computational procedure

In outline, the optics evaluation procedure consists of the following steps, using the program MAD [1] for the optical calculations:

- The optics, nominal beam energy, detailed RF configuration and any other conditions or parameters defining the machine configuration are chosen.
- The linear betatron coupling introduced by the solenoids is corrected using the usual tilted quadrupoles.
- An ensemble of 30 imperfect machines are generated, with random field errors, tilts and misalignments applied to all magnetic elements. The experimental solenoids and the sliced-up quadrupoles embedded in their fields are given special treatment to ensure the proper correlations among their random displacements and tilts. The magnitudes of the random errors have been chosen to reflect the real tolerances in LEP; in previous studies they have produced a good statistical correspondence between the simulated machines and the well-optimised operational state of LEP
- "Collimators" are inserted in many elements in order to simulate the vacuum chamber for tracking.
- Electrostatic separators were not excited in this case.
- The average orbit in each machine is corrected down to an RMS, as measured in the pickups, of 0.6 mm in the horizontal plane and 0.4 mm in the vertical plane. All correctors are used and various tricks are applied to find the closed orbit. This helps to ensure that the machine is not declared unstable in cases where the closed orbit is merely hard to find. However no attempt is made to simulate the operational procedure of finding a "golden orbit".
- The vertical beta-functions β_y^* are corrected to their nominal values at each IP using a matching procedure similar to that applied in operation.
- The tunes of the positron beam are corrected to their nominal values using the QF and QD strings. The tunes of the electrons are different.
- Physically equivalent imperfect machines are constructed for the positrons and electrons (in MAD this step is not trivial). Optics and beam parameter calculations are carried out for each machine and the results are condensed into a database of *Mathematica* functions.
- A 4-dimensional dynamic aperture scan (usually with fairly low resolution in the spherical polar angles in action space) is carried out for each machine. As usual for LEP, the initial phase of synchrotron oscillations has to be scanned. Tracking is done with the deterministic part of synchrotron radiation in every element (so radiation damping and other effects arise naturally). The dynamic aperture surfaces are also saved in the database. In the present study, the dynamic apertures were computed only for the positrons.

- Some machines can be selected for further study by, e.g., quantum tracking or analysis of particle loss mechanisms. These aspects are not discussed here.

The entire sequence of calculations, including the preparation, execution and analysis of the many MAD runs was carried out entirely within the medium of *Mathematica* notebooks [2]. The present summary report is itself a notebook set up to respect traditional formatting conventions in its printed version (e.g., all the input cells are hidden). The full interactive document contains the input expressions that generated all the results given above plus additional hyperlinked information. It is available from my WWW pages [3]. It can be used as a starting point for further study of the database of information on the imperfect machines.

1.2 Differences with the operational optics

It is natural to ask to what extent the optics used for the present study can be compared with the EBv1 optics that was tested in operation. This subsection provides the technical details for those who are interested.

The calculations were started around 13 October 1997, before the final version of the EBv1 optics was available, on a preliminary version which had linear matching by A. Verdier and a chromaticity correction (with the "re-cabled" configuration of 2 sextupole families per plane) by M. Lamont. In fact the linear optics differ only by a small re-distribution of betatron phase around IP2 and IP6. The phases at the ends of all insertions and, therefore, everywhere in the arcs are identical. Most nonlinear elements are located in the arcs. At high energy, where radiative beta-synchrotron coupling (RBSC) [4] is important, the superconducting quadrupoles must also be considered as nonlinear elements. The phases at these elements are also very close. The horizontal β -functions in IP4 and IP8 are slightly smaller in the EBv1 optics, alleviating the effects of RBSC.

The distribution of sextupole strengths in the arcs is somewhat different. In the EBv1 optics, the two horizontally focusing families are combined with the same strength ($KSSF1 = KSSF2 = 0.1902 \text{ m}^{-2}$). In the preliminary optics they have distinct values ($KSSF1 = .2308 \text{ m}^{-2}$, $KSSF2 = .1466 \text{ m}^{-2}$) some 20% higher and lower. The strengths of the D-sextupoles are practically the same.

A collection of plots and tables showing the differences between the optics in some detail is available in:

`/afs/cern.ch/user/j/jowett/public/lep97/mu10290/CompareOptics.nb`

Given the length of the calculations described in the following, it was not considered worthwhile to repeat them for the sake of these small changes. Should the four-parameter sextupole correction of the preliminary optics prove to be better, it can always be used in future.

2 Remarks on the results

As usual, it was possible to find and correct the average closed orbit for all 30 machines. However, when the RF cavities and radiation effects were switched on, MAD failed to find a closed orbit for 3 (i.e., 10 %) of the machines, even after some additional tricks were brought to bear. This is unusual in that the basic procedure found closed orbits for all the other optics studied recently. The results on damping partition numbers in the stable machines (see below) suggest that the mainly-vertical mode may be radiation anti-damped in the unstable machines.

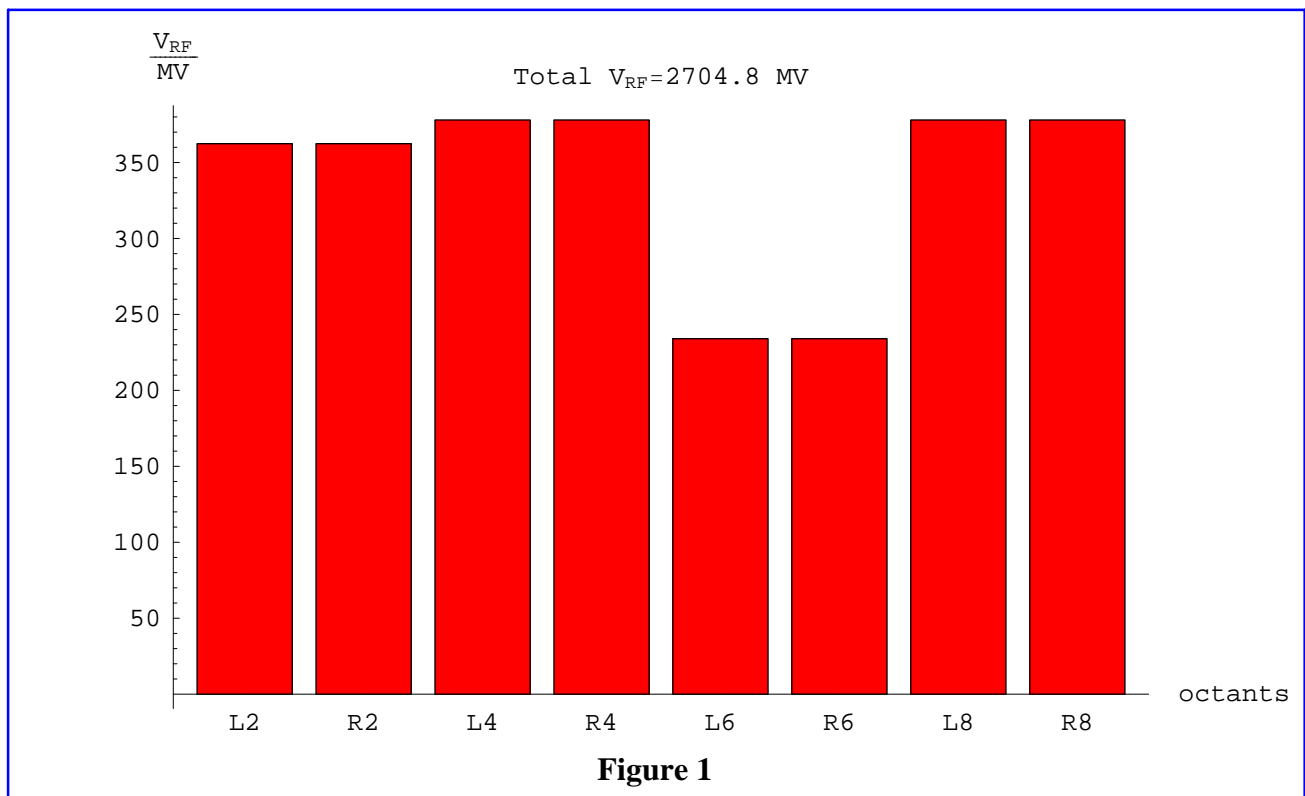
In the following, the means, standard deviations and other statistical quantities refer to the distribution of quantities over the ensemble of 27 machines for which a closed orbit was found. The

estimator for standard deviation quoted is always unbiased although it could be argued that a maximum-likelihood estimate (10% smaller here) would be justified for some physical quantities

Because of the strong radiation effects, the orbit and optics are different for the two beams. Therefore many quantities are given for both electrons and positrons. Some quantities, such as the tune splits or centre-of-mass energies, have to be derived by combining properties of the two beams.

3 RF configuration

It was assumed, rather idealistically, that each superconducting RF unit provided a peak voltage of 42 MV and each copper one 2.2 MV and that all units were properly phased. The 1997 configuration resulted in the distribution of RF voltage by octant of LEP shown in Figure 1. The total voltage is more than the minimum necessary [5,6] for the beam energy.



4 Orbits and optics

The imperfections of each machine in the ensemble give rise to different closed orbits after correction. Furthermore, in a given machine, the positrons and electrons, despite seeing the same imperfections, move in opposite directions around the ring. Since the terms in their equations of motion describing synchrotron radiation are not time-reversal invariant, they have very different closed orbits (separated horizontally by several mm in some places). The optical functions codify the behaviour of small displacements from these closed orbit and these, too, will differ from machine to machine and from one beam to the other. This section summarises the statistical information on orbits, optical functions and derived quantities such as the separations at the interaction points (IPs).

4.1 Global optical parameters

Table 1 lists the statistics for a number of global quantities related to the optics. Some of these are derived from the traditional Courant-Snyder (labelled "CS" in the table) calculations and may not take proper account of the radiation and RF effects but still have some indicative value. The tunes quoted are the correct tunes on the 6-dimensional closed orbit.

Quantity	Symbol	Mean	σ_{est}	Units
Momentum compaction for e^+	α_c^+	0.0001558	1.58×10^{-8}	
Momentum compaction for e^-	α_c^-	0.0001558	1.58×10^{-8}	
Max. horizontal CS β -function for e^+	$\beta_x^{\text{max}+}$	356.4	11.8	m
Max. horizontal CS β -function for e^-	$\beta_x^{\text{max}-}$	354.2	16.	m
Max. vertical CS β -function for e^+	$\beta_y^{\text{max}+}$	423.4	3.8	m
Max. vertical CS β -function for e^-	$\beta_y^{\text{max}-}$	425.6	4.08	m
Horizontal tune for e^+	Q_1^+	0.2806	0.0000259	
Horizontal tune for e^-	Q_1^-	0.281	0.00172	
Vertical tune for e^+	Q_2^+	0.1986	0.0000455	
Vertical tune for e^-	Q_2^-	0.1996	0.000471	
Synchrotron tune for e^+	Q_3^+	0.1225	0.0000353	
Synchrotron tune for e^-	Q_3^-	0.1224	0.0000298	
Horizontal tune split	ΔQ_1^\pm	-0.00039960	0.00172	
Vertical tune split	ΔQ_2^\pm	-0.001052	0.000474	
Horizontal CS chromaticity for e^+	$Q_x'^{+}$	0.9186	0.278	
Horizontal CS chromaticity for e^-	$Q_x'^{-}$	0.7614	0.297	
Vertical CS chromaticity for e^+	$Q_y'^{+}$	0.5681	0.148	
Vertical CS chromaticity for e^-	$Q_y'^{-}$	0.3028	0.133	
Horizontal chromaticity split	$\Delta Q_x'^{\pm}$	0.1572	0.093	
Vertical chromaticity split	$\Delta Q_y'^{\pm}$	0.2653	0.103	

Table

Since the tune correction for each machine was done on the positrons, the tunes of the positron beams have a very small spread while the electrons are left with a certain spread. The vertical tune-split is relatively small, thanks to the fairly symmetric RF voltage distribution.

4.2 Global orbits

Table 2 gives some global orbit parameters, where notations like $\overline{x^2}$ denote averages around the ring. The *average* $e^+ e^-$ orbit was corrected to 0.6 and 0.4 mm RMS in the horizontal and vertical planes. The larger RMS values for individual beams in the horizontal plane reflect the energy-sawtoothing.

Quantity	Symbol	Mean	σ_{est}	Units
RMS horizontal orbit for e^+	$\sqrt{\overline{x^2}^+}$	1.379	0.035	mm
RMS horizontal orbit for e^-	$\sqrt{\overline{x^2}^-}$	1.387	0.04	mm
Max. horizontal orbit for e^+	x_{max}^+	6.196	0.734	mm
Max. horizontal orbit for e^-	x_{max}^-	6.284	0.726	mm
RMS vertical orbit for e^+	$\sqrt{\overline{y^2}^+}$	0.3521	0.0189	mm
RMS vertical orbit for e^-	$\sqrt{\overline{y^2}^-}$	0.3575	0.0276	mm
Max. vertical orbit for e^+	y_{max}^+	1.441	0.147	mm
Max. vertical orbit for e^-	y_{max}^-	1.468	0.163	mm

Table

4.3 Orbits and separations at the interaction points

More detailed information about the orbits at the interaction points is given in Table 3.

Quantity	Symbol	Mean	$\sigma(\text{est})$	Units
Horizontal orbit for e^+ [IP2]	$x(\text{IP2})^+$	-0.02272	0.168	mm
Horizontal orbit for e^- [IP2]	$x(\text{IP2})^-$	-0.008959	0.163	mm
Horizontal orbit for e^+ [IP4]	$x(\text{IP4})^+$	-0.0009014	0.178	mm
Horizontal orbit for e^- [IP4]	$x(\text{IP4})^-$	-0.01679	0.18	mm
Horizontal orbit for e^+ [IP6]	$x(\text{IP6})^+$	-0.01396	0.198	mm
Horizontal orbit for e^- [IP6]	$x(\text{IP6})^-$	0.01384	0.196	mm
Horizontal orbit for e^+ [IP8]	$x(\text{IP8})^+$	0.01107	0.174	mm
Horizontal orbit for e^- [IP8]	$x(\text{IP8})^-$	-0.007141	0.168	mm
Horizontal separation [IP2]	$\Delta x^+ [\text{IP2}]$	-0.01376	0.0426	mm
Horizontal separation [IP4]	$\Delta x^+ [\text{IP4}]$	0.01589	0.0442	mm
Horizontal separation [IP6]	$\Delta x^+ [\text{IP6}]$	-0.0278	0.0459	mm
Horizontal separation [IP8]	$\Delta x^+ [\text{IP8}]$	0.01821	0.0444	mm
Vertical orbit for e^+ [IP2]	$y(\text{IP2})^+$	-0.002909	0.0262	mm
Vertical orbit for e^- [IP2]	$y(\text{IP2})^-$	-0.003486	0.0261	mm
Vertical orbit for e^+ [IP4]	$y(\text{IP4})^+$	-0.04421	0.118	mm
Vertical orbit for e^- [IP4]	$y(\text{IP4})^-$	-0.04432	0.118	mm
Vertical orbit for e^+ [IP6]	$y(\text{IP6})^+$	-0.02165	0.137	mm
Vertical orbit for e^- [IP6]	$y(\text{IP6})^-$	-0.02194	0.137	mm
Vertical orbit for e^+ [IP8]	$y(\text{IP8})^+$	0.01696	0.13	mm
Vertical orbit for e^- [IP8]	$y(\text{IP8})^-$	0.01651	0.131	mm
Vertical separation [IP2]	$\Delta y^+ [\text{IP2}]$	0.0005773	0.00201	mm
Vertical separation [IP4]	$\Delta y^+ [\text{IP4}]$	0.0001081	0.00218	mm
Vertical separation [IP6]	$\Delta y^+ [\text{IP6}]$	0.0002887	0.00157	mm
Vertical separation [IP8]	$\Delta y^+ [\text{IP8}]$	0.0004573	0.00172	mm

Table

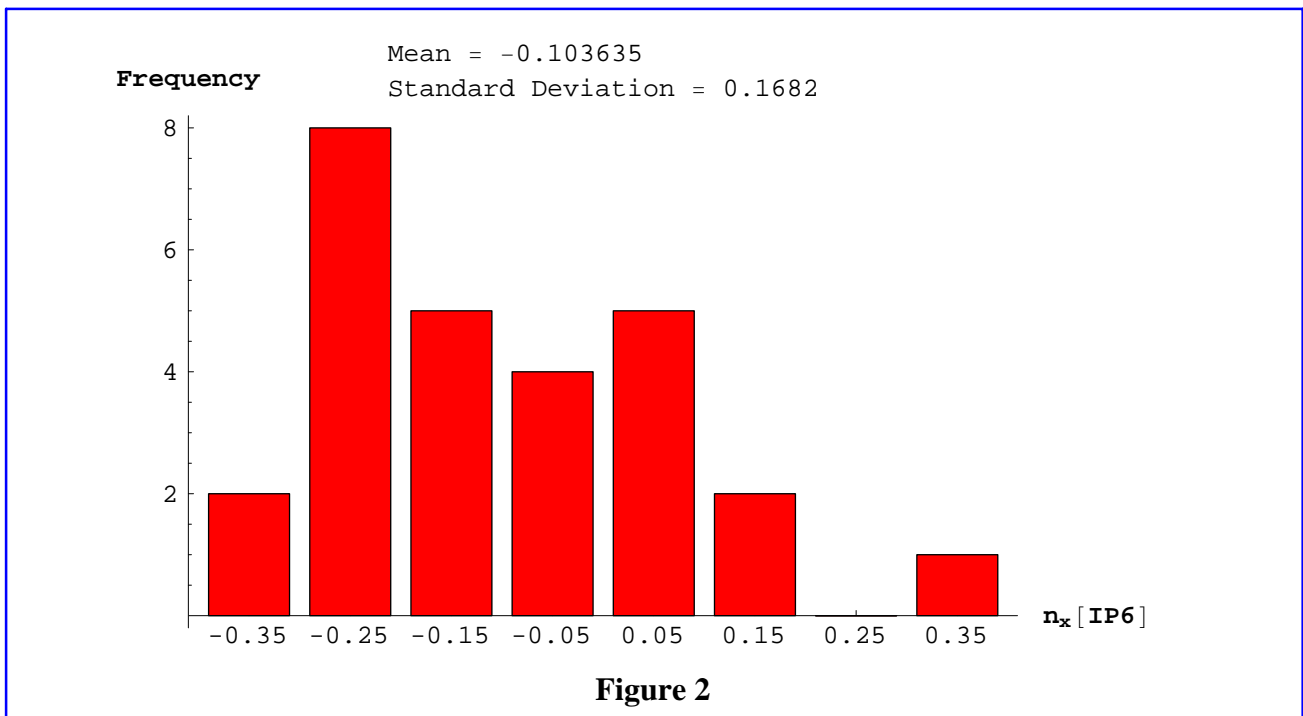
As usual in LEP, there are small horizontal and vertical separations at the interactions points. In operation the essentially random (zero mean) vertical separations are usually removed with

electrostatic separators. No separators are available in the horizontal plane. However if we express the separation in units of the beam size

$$n_x \approx \frac{\Delta x^\pm}{\sqrt{\beta_{x1}^\pm \varepsilon_{1^\pm}}}, \quad n_y \approx \frac{\Delta y^\pm}{\sqrt{\beta_{x1}^\pm \varepsilon_{1^\pm}}} \quad (1)$$

The largest horizontal separations actually occur in IP6 and are distributed according to the histogram in Figure 2.

It is clear that these are not worth correcting when compared with the beam size. They may however increase if RF units trip [7].



4.4 Optical functions at the interaction points

Table 4 gives the statistics for the β -functions in the interaction points. Each machine in the ensemble has had its vertical β -function corrected by a procedure that mimics the one followed in operation. The values for the imperfect machine are "measured" after orbit correction. A matching calculation is carried out using the ideal machine model to find increments of the QS0 quadrupoles that would produce these values. The negatives of these increments are then applied to the quadrupoles.

Quantity		Mean	σ (est)	Units
Horizontal β -function for e^+ [IP2]	β_{x1} (IP2) ⁺	2.	0.0983	m
Horizontal β -function for e^- [IP2]	β_{x1} (IP2) ⁻	2.007	0.102	m
Horizontal β -function for e^+ [IP4]	β_{x1} (IP4) ⁺	2.07	0.12	m
Horizontal β -function for e^- [IP4]	β_{x1} (IP4) ⁻	1.967	0.119	m
Horizontal β -function for e^+ [IP6]	β_{x1} (IP6) ⁺	1.962	0.102	m
Horizontal β -function for e^- [IP6]	β_{x1} (IP6) ⁻	1.944	0.0994	m
Horizontal β -function for e^+ [IP8]	β_{x1} (IP8) ⁺	1.925	0.0896	m
Horizontal β -function for e^- [IP8]	β_{x1} (IP8) ⁻	2.027	0.0935	m
Vertical β -function for e^+ [IP2]	β_{y2} (IP2) ⁺	0.05362	0.000589	m
Vertical β -function for e^- [IP2]	β_{y2} (IP2) ⁻	0.05169	0.000601	m
Vertical β -function for e^+ [IP4]	β_{y2} (IP4) ⁺	0.05171	0.00031	m
Vertical β -function for e^- [IP4]	β_{y2} (IP4) ⁻	0.04908	0.000814	m
Vertical β -function for e^+ [IP6]	β_{y2} (IP6) ⁺	0.05047	0.000338	m
Vertical β -function for e^- [IP6]	β_{y2} (IP6) ⁻	0.05168	0.00102	m
Vertical β -function for e^+ [IP8]	β_{y2} (IP8) ⁺	0.05257	0.00135	m
Vertical β -function for e^- [IP8]	β_{y2} (IP8) ⁻	0.05552	0.00119	m

Table

In this instance, a small error crept into the procedure: IP8 was corrected on the basis of the values measured in IP6. Since this was done at an early stage of very lengthy calculations but did not appear to produce any very detrimental effects on other quantities, the error was not corrected. The following Figure 3 shows the resulting correlations of vertical β -functions between beams in each IP. The coordinates of each point are given by the β -functions of the positron and electron. The four clouds of points represent the values at each IP.

The error in this correction cannot be invoked as a possible explanation of the 10% of machines that were "unstable" (see Section 2) because the same error was present in previous Monte-Carlo treatments of other optics (although it could conceivably enhance the differences between optics).

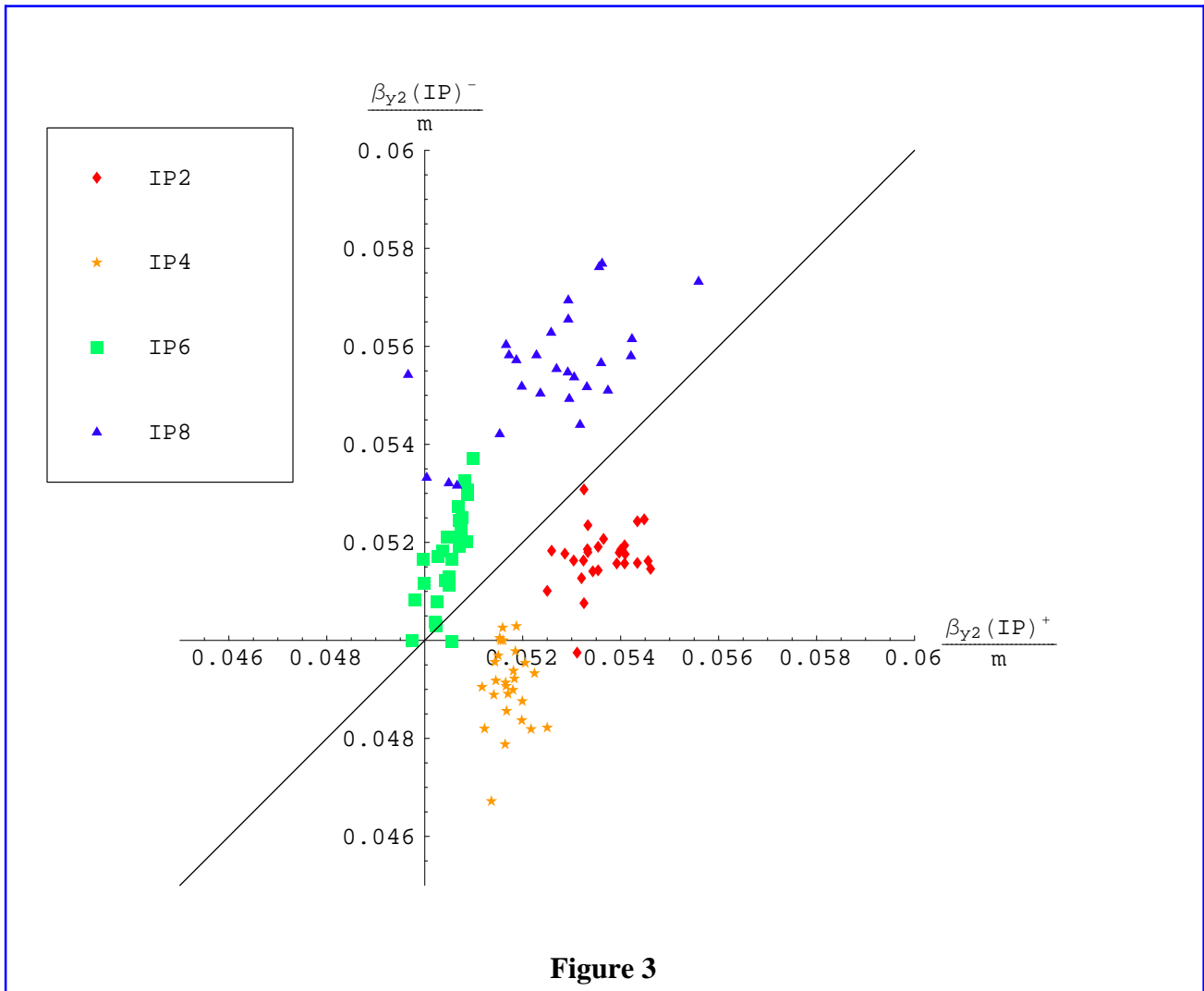


Figure 3

5 Parameters of the beams

As a further consequence of the different orbits and optics among machines and between beams in a given machine, beam parameters determined by integrals along the 6-dimensional closed orbit can differ. This section summarises the statistical information for some of the most important beam parameters.

5.1 Energy loss and radiation damping

Table 5 is a summary of the values of selected parameters related to the energy lost by synchrotron radiation and the radiation damping. The energy lost per turn is slightly higher than the 2049.2 MeV given by the standard calculation [5,6] using synchrotron radiation integrals for a particle with constant nominal energy on the central trajectory passing through the centres of the elements. The additional 2 MeV of energy is lost as the closed orbit passes off-centre through quadrupoles and other elements because of energy sawtoothing and the imperfections.

The damping partition numbers are close to their nominal values, except in the vertical mode. The correlation plot between damping partition numbers for the two beams is shown in Figure 4.

Quantity	Symbol	Mean	σ (est)	Units
Beam energy for e^+	E_b^+	91.5	0.	GeV
Beam energy for e^-	E_b^-	91.5	0.	GeV
Average momentum deviation for e^+	δ_s^+	0.	0.	
Average momentum deviation for e^-	δ_s^-	0.	0.	
Energy loss per turn for e^+	U_0^+	2051.	0.231	MeV
Energy loss per turn for e^-	U_0^-	2051.	0.269	MeV
Horizontal damping partition for e^+	J_1^+	1.007	0.0163	
Horizontal damping partition for e^-	J_1^-	1.011	0.0153	
Vertical damping partition for e^+	J_2^+	0.97	0.045	
Vertical damping partition for e^-	J_2^-	0.9604	0.0652	
Longitudinal damping partition for e^+	J_3^+	2.023	0.0447	
Longitudinal damping partition for e^-	J_3^-	2.029	0.0605	
Horizontal damping time for e^+	τ_1^+	0.007881	0.000126	sec
Hor. damping time in turns for e^+	τ_1^+ / T_0^+	88.63	1.42	
Vertical damping time for e^+	τ_2^+	0.008196	0.000402	sec
Vert. damping time in turns for e^+	τ_2^+ / T_0^+	92.17	4.52	
Longitudinal damping time for e^+	τ_3^+	0.003923	0.0000849	sec
Long. damping time in turns for e^+	τ_3^+ / T_0^+	44.12	0.955	

Table

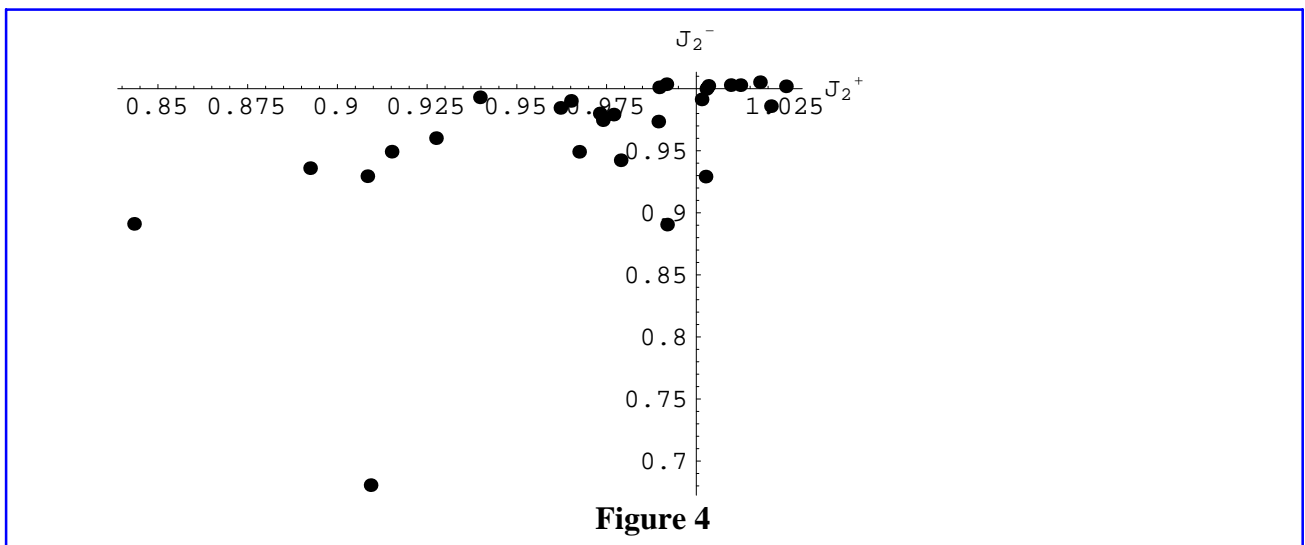


Figure 4

It can be seen from the following Figure 5 that there is a significant correlation between the shift in the damping partition number and the RMS vertical dispersion around the ring. The change can be produced in strong quadrupoles where there is a combination of vertical orbit *and* dispersion.

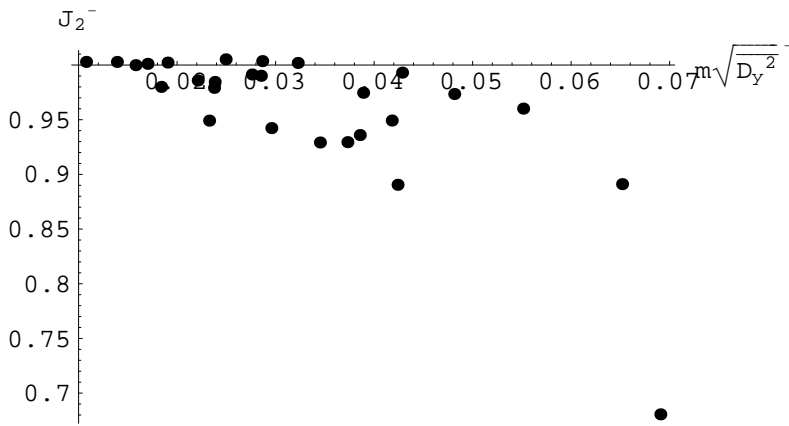


Figure 5

5.2 Centre-of-mass energy in collision

Knowing the values of the canonical momenta p_t^+, p_t^- (as defined by MAD Version 8 [1]) on the closed orbits of the two beams, and neglecting terms involving the mass of the electron, the centre-of-mass (CM) energy in collisions is given by

$$w = 2 \left(E_0^+ E_0^- (p_t^- + 1) (p_t^+ + 1) + \sqrt{(E_0^-)^2 (p_t^- + 1)^2 - m_e^2} \sqrt{(E_0^+)^2 (p_t^+ + 1)^2 - m_e^2} \right)^2 + 2 m_e^2 \quad (2)$$

$$\approx 4 E_0^+ E_0^- (p_t^- + 1) (p_t^+ + 1) - (E_0^+ / E_0^- - E_0^- / E_0^+) m_e^2$$

where the second form includes terms up to second order in the small quantities $\frac{m_e}{E_0}, p_t^-, p_t^+$. Usually the nominal beam energies are equal and the approximate form simplifies to:

$$w = 4 E_0^2 (p_t^- + 1) (p_t^+ + 1) \quad (3)$$

but we shall always use the exact form in the following.

At IP2 for example, the prepared ensemble of imperfect machines has a distribution of CM energies. This can be expressed as a deviation in MeV from the nominal 183 GeV as in Figure 6.

Imperfections in the present Monte-Carlo simulations indicate possible drifts of machine conditions over an operating period due to the effects included. They do not include other external trends in the machine conditions. With these caveats, the expected variation is of the order of 5 MeV.

The CM energies may differ from one experiment to another, mainly because of the RF voltage distribution. The 4 data sets in Figure 7 are the shift in CM energies at each IP. To make the plot clearer, the machines have been sorted according to the CM energy in IP6. The horizontal axis is just the resulting indexing of the machines.

The correlations in the ensemble of prepared machines are clear from this plot: the CM energy in IP6 is systematically lower than in the other IPs by about 1.6 MeV.

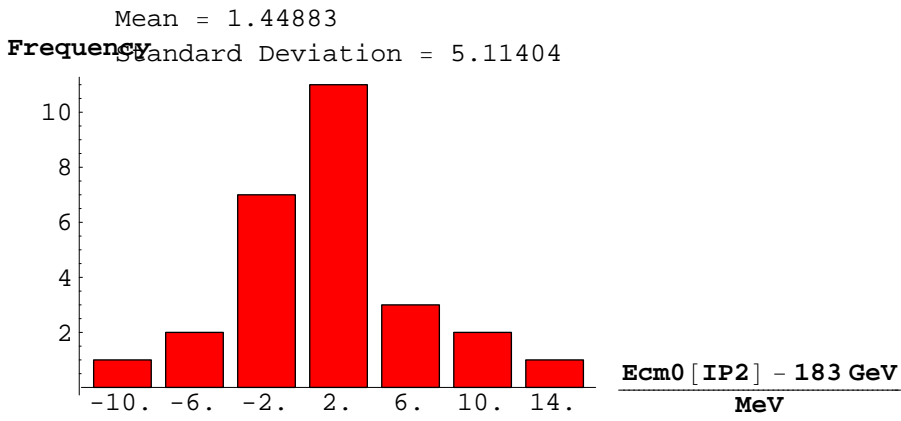


Figure 6

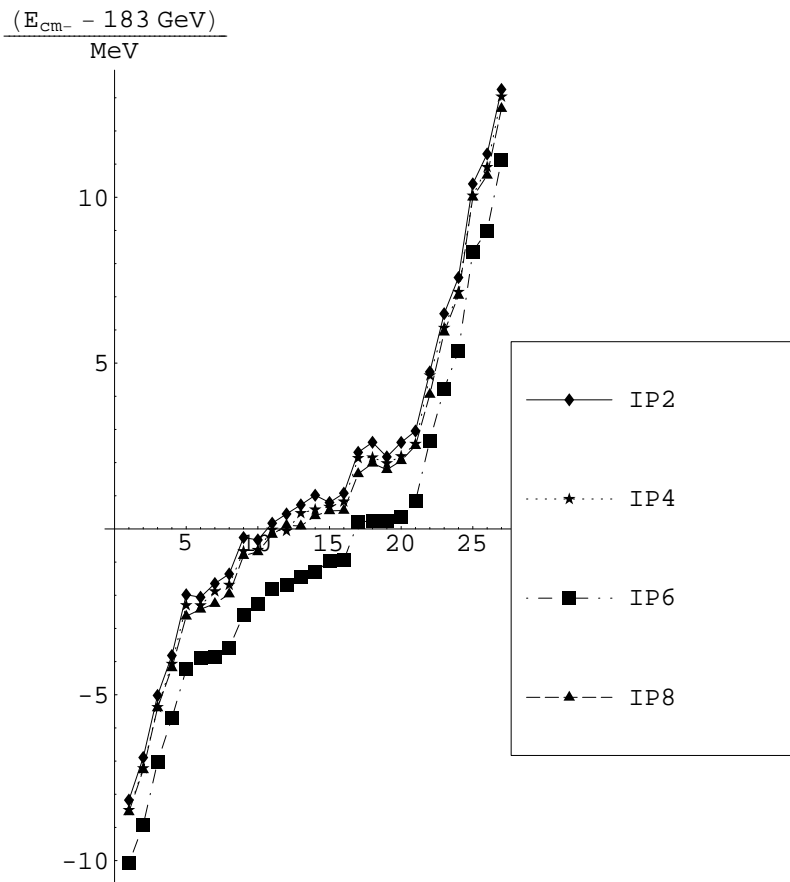


Figure 7

5.3 Emittances and energy spread

Table 6 summarises the distributions of the emittances and related quantities. The horizontal emittance has a rather small spread about its nominal value.

Quantity	Symbol	Mean	σ (est)	Units
Horizontal emittance for e^+	ε_1^+	38.08	0.986	nm
Horizontal emittance for e^-	ε_1^-	37.91	0.758	nm
Vertical emittance for e^+	ε_2^+	0.4943	0.368	nm
Vertical emittance for e^-	ε_2^-	0.5183	0.444	nm
Fractional energy spread for e^+	σ_{ε^+}	0.0014330	0.0000156	
Fractional energy spread for e^-	σ_{ε^-}	0.0014310	0.0000202	
Bunch length for e^+ [IP2]	$\sigma_z(\text{IP2})^+$	0.0077460	0.0000841m	

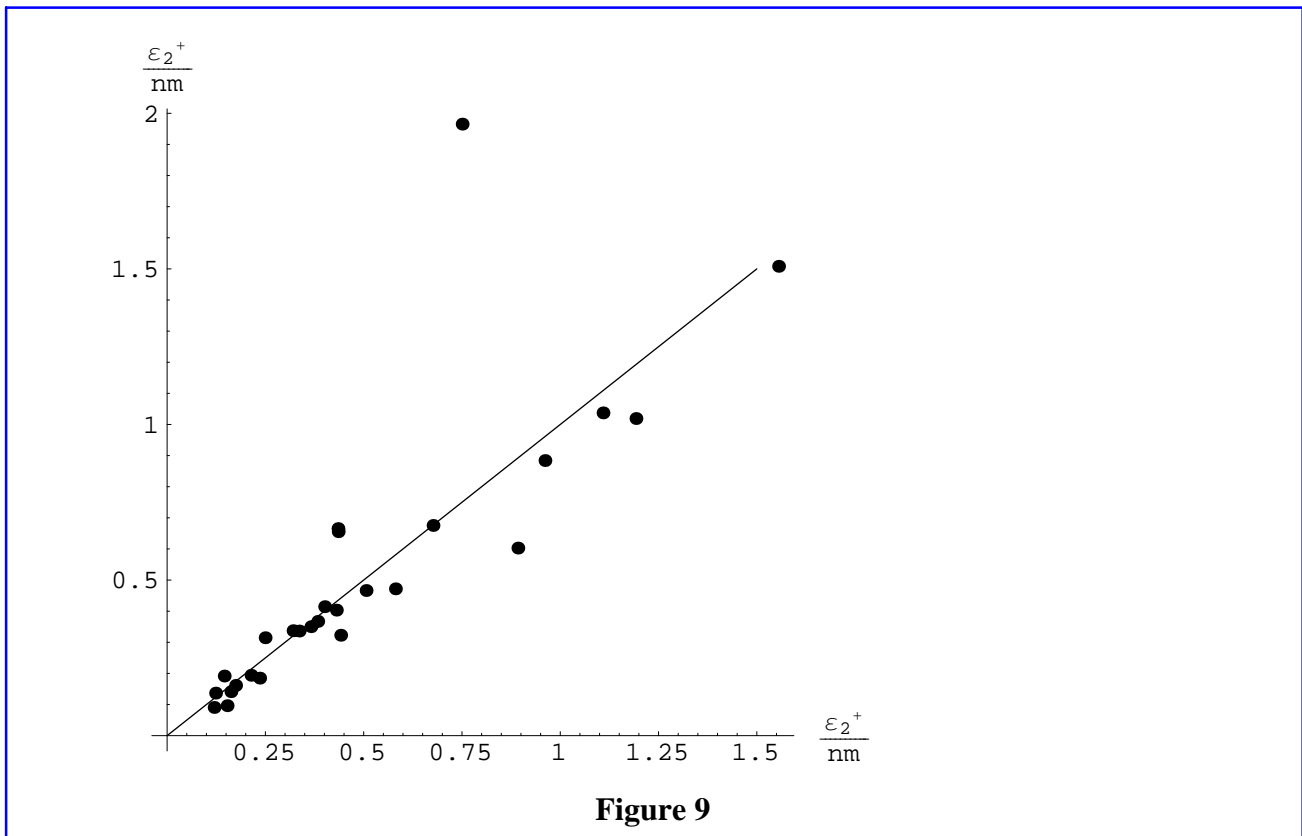
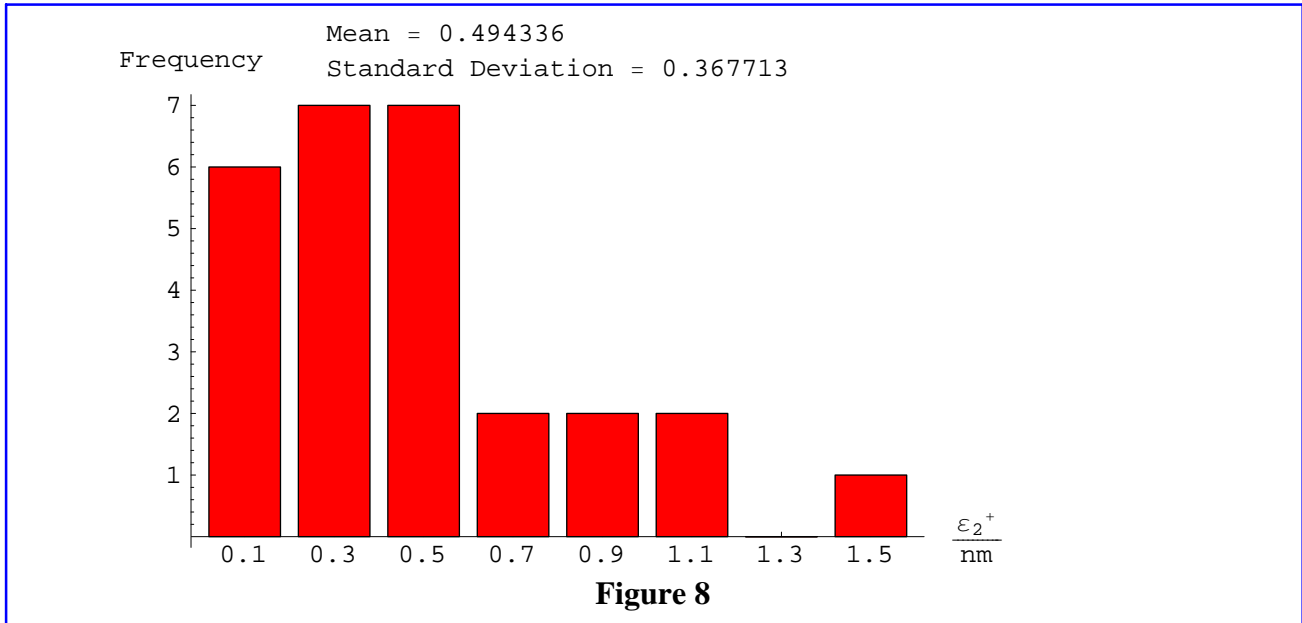
Table

The emittance ε_2 of the mainly-vertical mode is critical for the performance of the machine. The present simulation includes most optical effects that generate it (except the electrostatic separation bumps) but it should be kept in mind that the emittances given in Table 6 are the result of a *linear* eigenvector calculation. Roughly speaking, the linear vertical emittance has two components:

- The vertical emittance generated by linear coupling. This includes the transverse betatron coupling generated by solenoids and skew-quadrupole fields and the linear synchro-betatron coupling generated by dispersion at RF cavities).
- The intrinsic vertical emittance generated by quantum excitation in locations where there is a magnetic field and a non-zero value of the optical function β_{y3} (or "dispersion"). The contribution of this effect to the emittance is inversely proportional to the vertical damping rate.

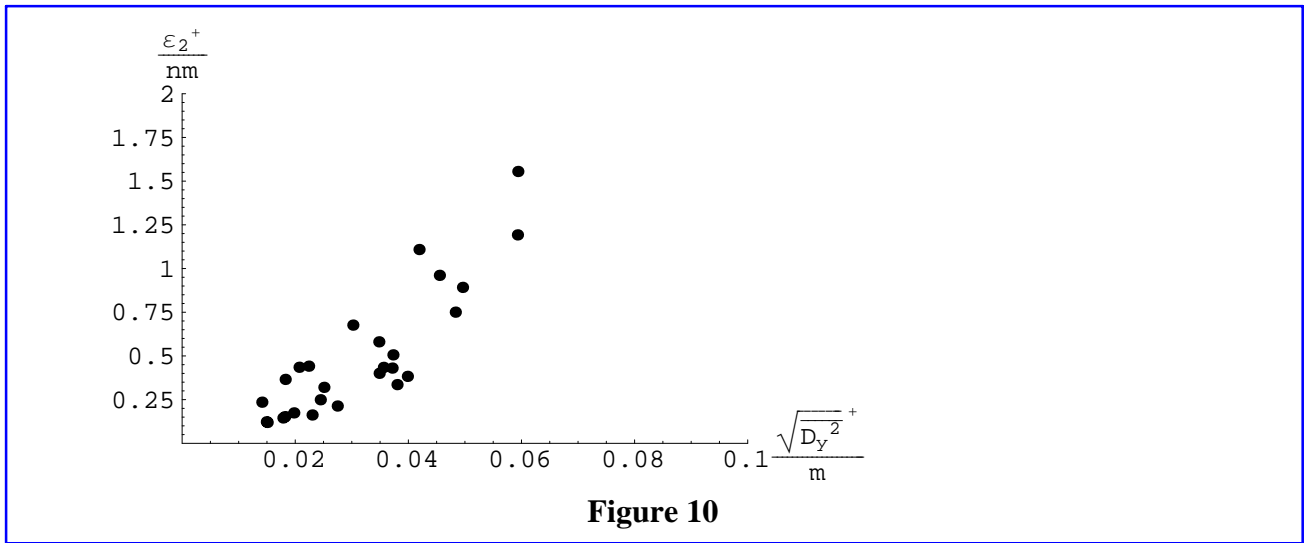
It has been shown [8] that the true vertical emittance may be larger than given by the linear calculation because of nonlinear effects. The calculations are beyond the scope of the present report and will be reported on elsewhere.

Apart from a single outlying machine in the ensemble, the emittances of the positrons and electrons are rather well-matched (see Figure 9, in which the solid line is the diagonal $x = y$, not a fit).



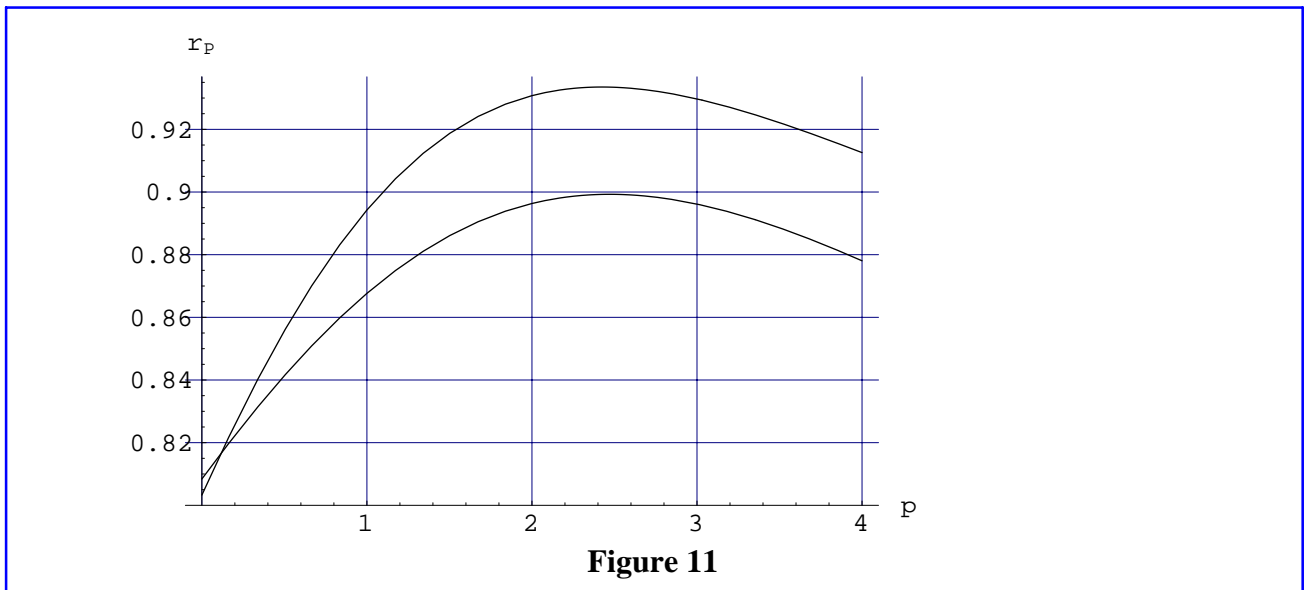
Since $\varepsilon_2 \propto \langle D_y^2 \rangle / J_2$, one would expect that some part of the distribution of vertical emittances can be attributed to the variation of the damping partition number of the mainly-vertical mode between machines (see Figure 4). However both the vertical quantum excitation and the damping partition depend on the vertical dispersion function (Figure 5). A plot of the vertical emittance against the RMS vertical dispersion, Figure 10, suggests a power-law behaviour

$$\varepsilon_2 \propto \overline{(D_y^2)}^{p/2} . \tag{4}$$



- Graphics -

To extract the power p , which we expect to be somewhat larger than 2, we can plot the Pearson correlation, r_p , between the left and right-hand sides of (4) as a function of p ; see Figure 11 and the Appendix. The two curves in Figure 11 are obtained from the positron and electron data.



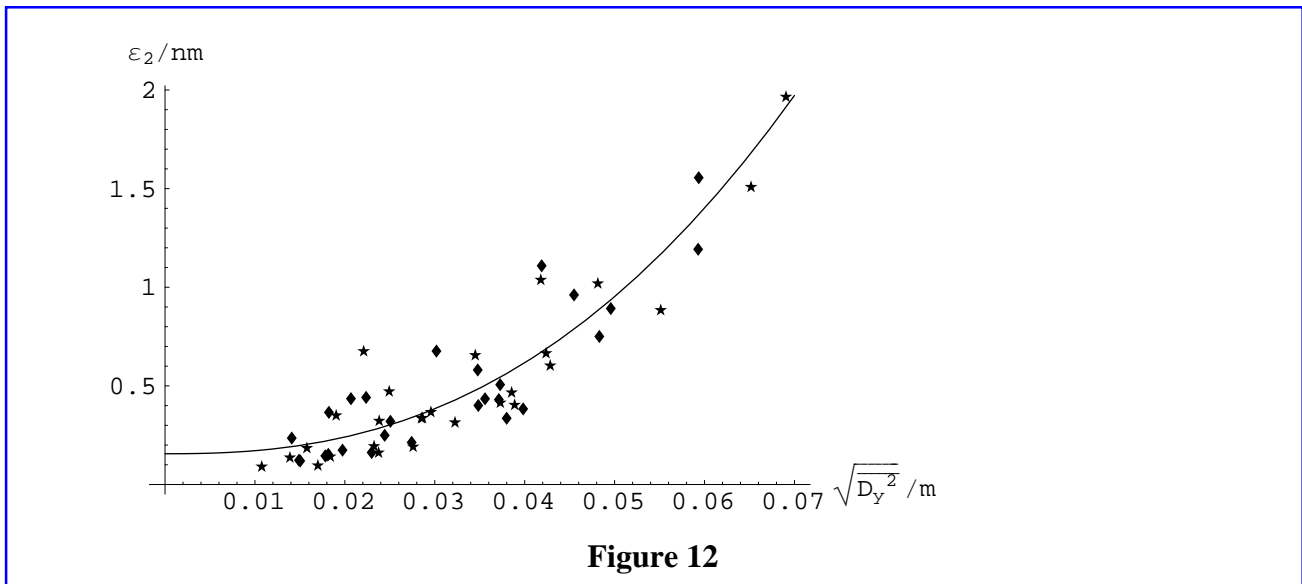
The maxima of the two curves occur at

$$p = 2.47108 \quad \text{and} \quad p = 2.42436 \tag{5}$$

and, taking the average of these two values, we can postulate an empirical formula for the vertical emittance in terms of the RMS vertical dispersion. A fit including a constant term to take account of residual betatron coupling gives

$$\frac{\varepsilon_2}{\text{nm}} = 1226.54 \left(\frac{D_y^{\text{rms}}}{\text{m}} \right)^{2.45} + 0.155989 \quad (6)$$

and this is plotted, together with the data for both beams in Figure 12. This formula is to be interpreted in a statistical sense. It may well be that the vertical emittance is particularly sensitive to the values of the vertical dispersion function in certain locations.



The numerical coefficient in (6) is appropriate for an RMS vertical dispersion measured all around the ring - the numerical coefficient will be different for an average restricted to the pickups.

6 Dynamic Aperture

Following some 45 years of tradition [9], the transverse dynamic apertures A_x, A_y are defined as the largest stable initial values of the "Courant-Snyder invariants". Although not invariants, these are just twice the action variables of the first two eigenmodes of linear oscillation (roughly speaking, the "horizontal and vertical betatron motion") about the 6-dimensional closed orbit and are expressed in metres. The emittances are the averages of the actions over the beam distribution. The projection of the dynamic aperture of the third mode ("synchrotron motion") is entirely analogous but is customarily converted to a dimensionless form in which its square root can be interpreted as the amplitude of a fractional momentum deviation in percent.

In LEP, it is convenient and has become customary to quote the *square roots* of the dynamic aperture projections rather than the quantities themselves.

The following summary table shows that this optics has a large dynamic aperture in the mainly-horizontal mode:

Quantity		Mean	σ (est)
Horizontal dynamic aperture	$10^3 \sqrt{A_x} / m$	2.741	0.277
Vertical dynamic aperture	$10^3 \sqrt{A_y} / m$	1.471	0.034
Longitudinal dynamic aperture	$\sqrt{A_t} / \%$	1.46	0.102

Table

The standard calculation [5,6] of the energy acceptance from the RF voltage predicts a longitudinal dynamic aperture of

$$\sqrt{A_t} = 0.0147834. \tag{7}$$

Given that the standard calculation underestimates the energy loss slightly, this is confirmation that the longitudinal dynamic aperture is indeed given by the RF voltage. That is, the chromaticity correction is adequate.

It is worth recalling here that, in order to evaluate the momentum acceptance correctly, it is essential to track particles with initial synchrotron phases scanned over the interval $[0, 2\pi)$. Failure to do this in the case of LEP can result in a momentum acceptance up to a factor of 2 too large. This is illustrated in Figure 13, a survival plot of particles tracked in the plane $A_y = 0$ for one particular machine in the ensemble. Black dots represent initial conditions of particles that survived to the end of the tracking (100 turns) and progressively lightening shades of grey indicate shorter survival times (of course this is better seen in colour). Although for certain initial phases, stable particles are found out to values of $\sqrt{A_t} > 0.03$, it is only when other phases are tracked that the true momentum acceptance (7) is found.

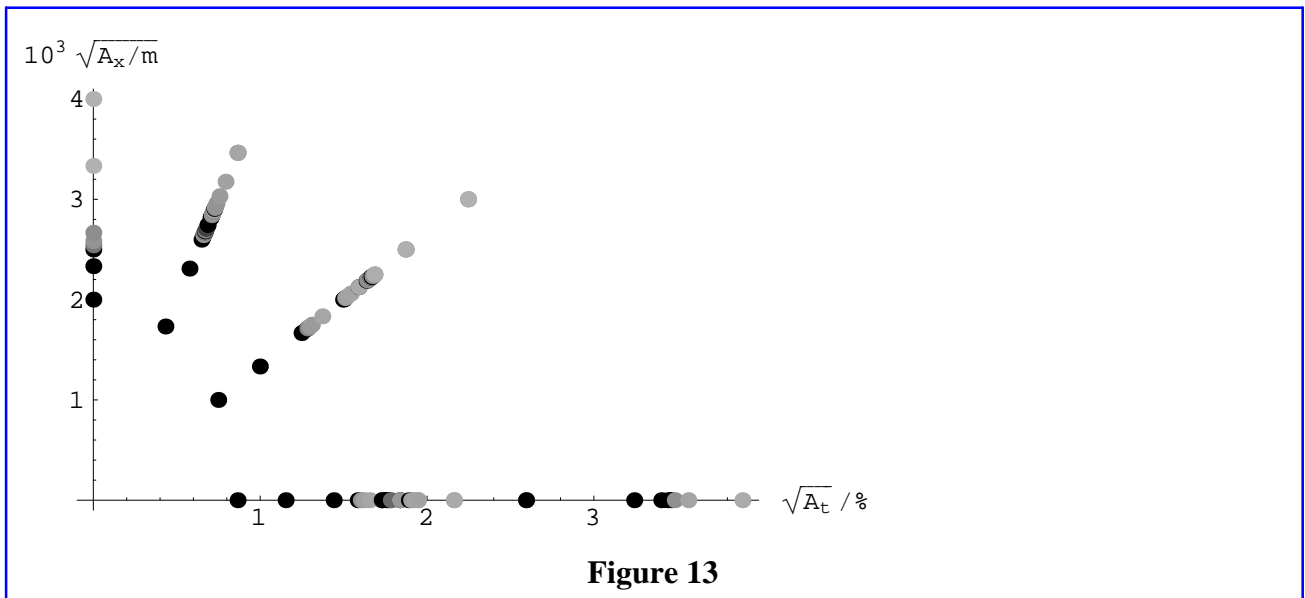


Figure 13

Figure 14 shows the survival plot in the particle amplitude space. In both these plots, the synchrotron phase dimension is "rolled-up" so that several points of varying synchrotron phase can be on top of each other. The number of particles tracked for this machine is 421.

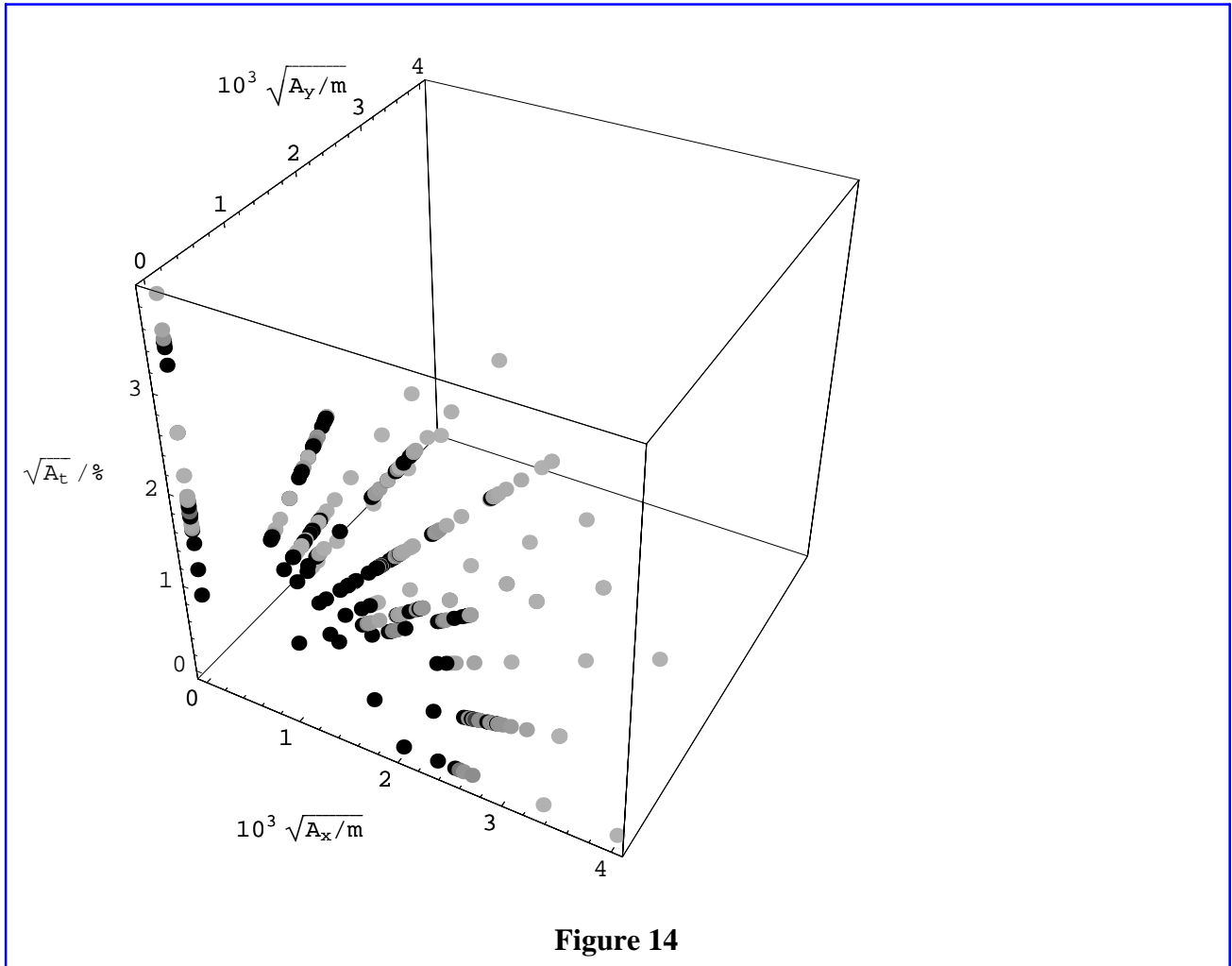
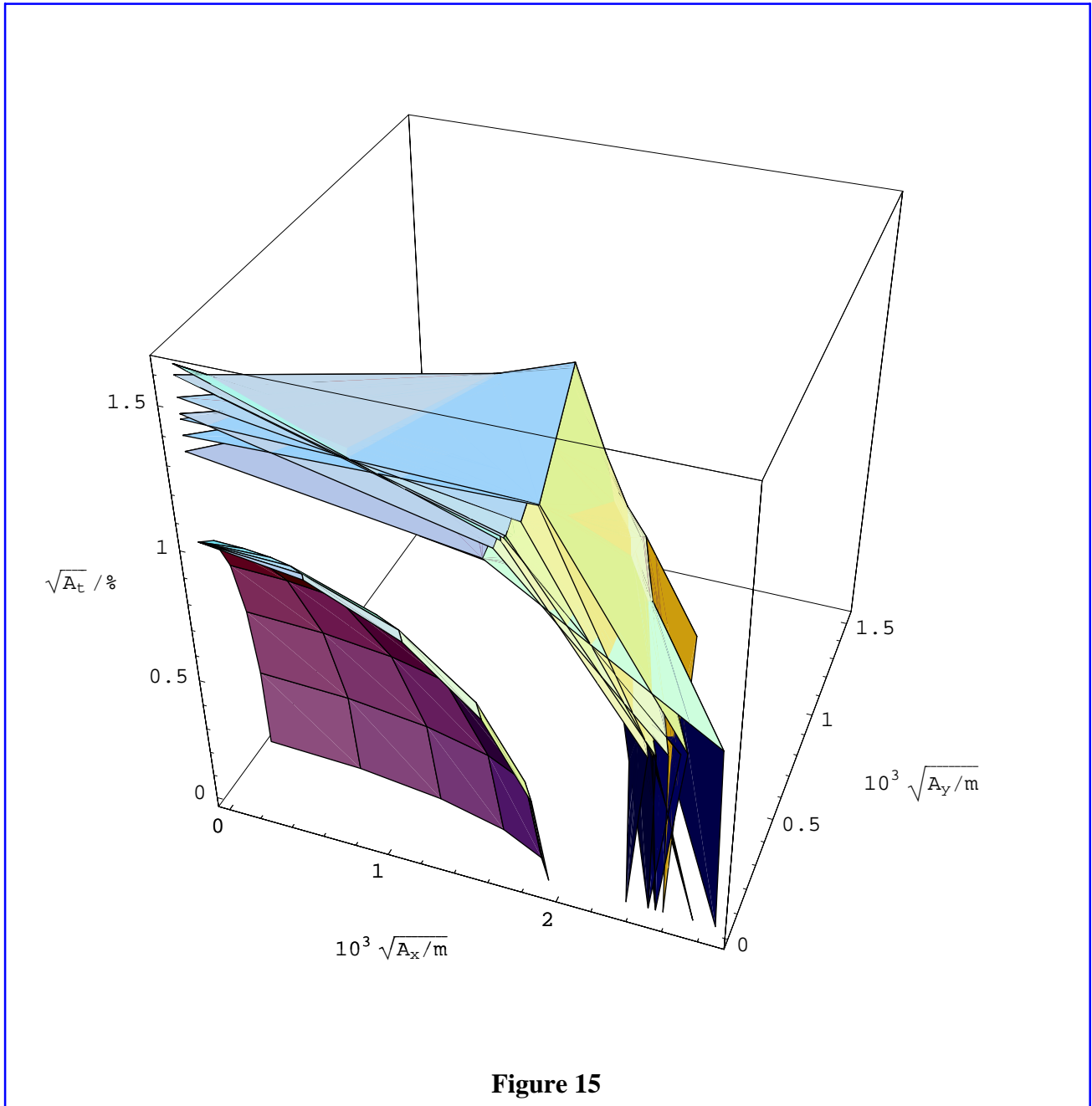


Figure 15 provides a graphical impression of the distribution of the 4D dynamic aperture surfaces projected into the space of amplitudes of the three normal modes. To avoid cluttering the figure too much, only the first 8 of the 27 dynamic apertures are shown. However they are quite representative of the full ensemble. The inner ellipsoidal surface has projections on the axes corresponding to $(10 \sigma_1, 10 \sigma_2, 7 \sigma_3)$ derived from the linear emittances. It is shown purely to indicate the scale of the dynamic aperture and plays no role in the calculation. The surface shown actually corresponds to the beam parameters of the third machine in the ensemble which happens to have $\varepsilon_2^+ = 0.58$ nm.



Note that the horizontal dynamic aperture has a significant spread in values. However the vertical dynamic aperture is sharply defined on the ensemble of machines (see Figure 16). Previous experience suggests that this is characteristic of a dynamic aperture limited by non-linear resonances at large amplitude. Detailed study of the phase space could test this hypothesis.

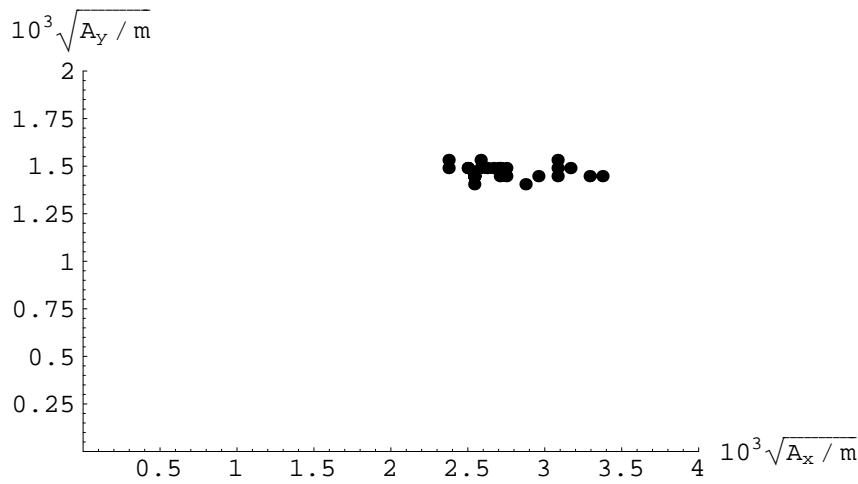


Figure 16

There is no particular correlation between the horizontal dynamic aperture and the momentum acceptance (Figure 17). Indeed further exploration of the database of imperfect machines reveals no particular correlations of dynamic aperture components with quantities such as the emittances, dispersions, tunes or chromaticities.

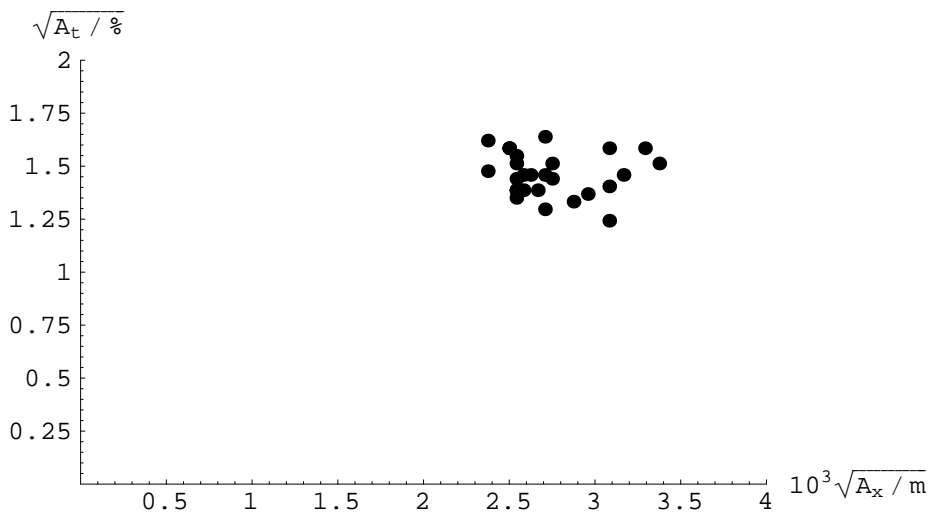


Figure 17

7 Conclusions

The Monte-Carlo procedure for evaluating an optical configuration shows that a LEP optics with $\mu_x = 102^\circ$ and $\mu_y = 90^\circ$ in the arc cells can be expected to perform well once the usual corrections are applied. The dynamic aperture is relatively large and the vertical emittance can be made small (at least in a linear calculation). The dominant component of the vertical emittance is generated by vertical quantum excitation since the linear betatron coupling is straightforwardly eliminated. However the calculations reported here should be supplemented by quantum tracking to evaluate possible nonlinear contributions to the vertical beam size. Further detailed studies of the effects limiting the dynamic aperture are also desirable.

When compared with other LEP optics given the same treatment, the only unusual feature is that some 10% of the imperfect machines generated were found to be unstable (in the sense that a closed orbit could not be found) when the RF cavities and radiation were switched on. The fact that a spread in the vertical damping partition number of the remaining machines is correlated with the vertical dispersion suggests that these machines were anti-damped.

Finally, it should be said that the computations reported here were carried out before and during the recent operational test of a very similar optics. While no attempt at detailed comparison has been made here, there is no indication of any substantial disagreement between the predictions and the operational experience once the machine was well tuned for physics.

7.1 Acknowledgements

Thanks to Mike Lamont for providing the optics files.

8 References

- [1] Hans Grote, F. Christoph Iselin, The MAD Program, User's Reference Manual, CERN/SL/90-13 (AP), and <http://wwwslap.cern.ch/~fci/mad/mad.html>
- [2] Stephen Wolfram, *The Mathematica Book*, 3rd ed., Wolfram Media/Cambridge University Press, 1996.
- [3] <http://wwwslap.cern.ch/~jowett/JMJdocs.html>
- [4] J.M. Jowett, *Dynamic Aperture for LEP: physics and calculations*, in J. Poole (Ed.), Proc. 4th LEP Performance Workshop, CERN SL/94-06 (DI).

In various places, comparisons have been made with the results of standard beam parameter calculations using the well-known formulas [6] that neglect the effects of energy-sawtoothing and imperfections on the orbit and optics. These are implemented, for example, in the program WIGWAM and a set of results corresponding to the conditions of the present simulations can be found at

- [5] <http://wwwslap.cern.ch/~jowett/lep97/mu10290/mu10290by5A.wigout>

- [6] M. Sands, *The Physics of Electron Storage Rings*, SLAC-121 (1970).

[7] J.M. Jowett, *Effects of an RF Trip in a Perfect LEP2*, CERN LEP2 Note 94-17 (1994) .

J.M. Jowett, *Non-linear Resonances: Predictions, Effects and Measurements*, in J. Poole
 [8] (Ed.), Proc. Seventh LEP Performance Workshop, Chamonix, January 1997,
 CERN-SL/96-06 (1997).

[9] T. Sigurgeirsson, CERN Report CERN-T/TS/2 (1952). See also E.D. Courant and H.S.
 Snyder, Ann. Phys. **3** (1958) 1.

W.H. Press, B.P. Flannery, S.A. Teukolsky, W.T. Vetterling, *Numerical Recipes, The Art*
 [10] *of Scientific Computing*, Cambridge University Press, Cambridge, 1986, and
<http://cfata2.harvard.edu/nr/>

[11] Wolfram Research, Inc., *Mathematica 3.0 Standard Add-on Packages*, Wolfram
 Media/Cambridge University Press, 1996.

9 Appendix: Statistical Significance of Correlations

Various physical parameters of an ensemble of imperfect machines can be correlated because there is some physical relationship between them. The correlation between a pair of variables $x = (x_1, \dots, x_N)$ and $y = (y_1, \dots, y_N)$ can be quantified by means of standard statistical quantities such as Pearson's r coefficient, r_P , [10] which describes the *linear* correlation between the variables. To cover cases where the correlation might not be linear but is nevertheless expected to be monotonic, I have also used the Spearman Rank Correlation, r_S , and the Kendall Rank Correlation coefficient, τ_K . The purpose of this Appendix is to recall some well-known facts about these measures and to explain how they have been used in the present study and, therefore, what it means when it is said that two variables are correlated or not. Further information can be found in [10] and [11] for example.

All three of these take values in $[-1, 1]$, with a value of zero representing a total lack of correlation, 1 a perfect positive correlation and -1 a perfect anti-correlation. In the case of r_P , the extreme values are realised when the data all lie on a straight line with positive or negative slope. In the case of the two rank correlations, the extreme values are realised if, when the data are sorted so that x is in increasing order, then y either increases or decreases monotonically.

However, since the sample size, N , used in these studies is not very large (typically 30, 27 in the present case), it is necessary to test any such correlation for its statistical significance against the null hypothesis that x and y are not correlated. In the case of Pearson's r_P , a standard method is to use the statistic

$$t_P = r_P \sqrt{\frac{N-2}{1-r_P^2}}, \quad (8)$$

which, in the case of the null hypothesis (no correlation) and a binormal distribution of (x, y) , can be expected to be distributed according to Student's t -distribution with $N-2$ degrees of freedom. Given a required significance level, typically $\xi=1\%$, the null hypothesis predicts that the probability of the observed value of t_P being greater than the observed value is given by the quantile of Student's t -distribution at $1-\xi$.

(Strictly speaking, this test only applies when the distribution of x and y is binormal or for very large N . However its use in other cases is justifiable: see [10]).

A similar test is applied to evaluate the significance of the Spearman rank correlation, r_S .

In the case of the the null hypothesis, the Kendall rank correlation, τ_K is expected to be distributed normally about a mean of zero with standard deviation [10]

$$\sigma(\tau_K) = \sqrt{\frac{4N + 10}{9N(N - 1)}} = 0.1367 \text{ for } N = 27. \quad (9)$$

Therefore the probability of observing a value deviating from zero by more than $|\tau_K|$ by pure chance is given by

$$\text{Erfc}\left[\frac{|\tau_K|}{\sqrt{2} \sigma(\tau_K)}\right]. \quad (10)$$

In the present study, these three tests have been applied to decide whether two variables are correlated. Taking the case of the vertical emittances of the two beams as an example, the results are quoted in the following format:

Correlations between Vertical emittance for e^+ and Vertical emittance for e^-
 Linear fit: $\epsilon_2^+ = 0.982 \epsilon_2^- + 0.0326$
 Pearson linear correlation $r_P =$
 0.814 IS NOT significant at $1. \times 10^{-7}$ level.
 Spearman rank correlation $r_S =$
 0.941 IS significant at $1. \times 10^{-7}$ level.
 Null hypothesis \Rightarrow Probability of Kendall rank correlation τ_K
 > 0.829 (observed) $< 1.31 \times 10^{-9}$

An extremely demanding significance level ($\xi = 10^{-7}$) has been chosen in this example, just in order to show that the three tests are not equivalent. In this case, the non-significance merely amounts to saying that the observed value of r_P might happen by accident once in 10 million repetitions of the calculations. In practice, I used a significance level of $\xi = 1\%$ or 0.1% .

10 INITIALISATION and other material that is not to be printed